Chapter 13

Modeling Aspects of Nonlinear Energy Harvesting for Increased Bandwidth

Marcus Neubauer, Jens Twiefel, Henrik Westermann and Jörg Wallaschek

Additional information is available at the end of the chapter

http://dx.doi.org/10.5772/52232

1. Introduction

Over the last years, the field of energy harvesting has become a promising technique as power supply of autonomous electronic devices. Those use the surrounding energy, such as vibrations, temperature gradients or radiation, for conversion in electrical energy. Mechanical vibrations are an attractive source due to their high availability in technical environments, thus numerous research groups are working on this topic. The most important conversion methods for ambient vibrations are electromagnetic, electrostatic and piezoelectric. All those techniques have been successfully demonstrated in the past. [11] provides an overview of the basics in energy harvesting.

Due to the fact, that vibration energy harvester generates the most energy when the generator is excited at its resonance frequency, the converter needs to be tuned to the main external frequency of the individual environment. If the excitation frequency shifts, the performance of the generator may reduced drastically. In practical use the vibration of an environment may vary in a large spectrum. To overcome this disadvantage researchers work hard to increase the working bandwidth of an energy harvester.

This chapter is a contribution to the current state of the art for modeling broadband energy harvesting generators. In the first part the electromechanical model is derived in terms of using lumped parameters. The system is based on a piezoelectric bimorph structure. The coupled differential equations for the case of a simple electrical circuit are derived and furthermore the possibility to enhance the energy extraction is analyzed. The use of generator arrays to archive a high power outputs in a wide frequency range is discussed. In detail, the Synchronized Switch Harvesting on Inductor (SSHI) technique is studied. Further the modeling of the promising piezomagnetoelastic energy harvesting technique is covered in the last part.

2. Linear piezoelectric energy harvesting system

This section is devoted to the modeling of a linear piezoelectric bimorph for energy harvesting. This will be the basis for the proposed nonlinear techniques with enhanced bandwidth duscussed in the following sections.

2.1. Modeling of piezomechanical structures

Fundamental for the energy harvesting techniques presented in the following is the piezoelectric bimorph. In the following, the general modeling of piezomechanical structures is given, and further on applied to the case of a bending bimorph.

The calculations are based on the potential energy stored in a piezoelement,

$$U = \frac{1}{2} \int_V \left(T_i S_i + D_3 E_3 \right) \mathrm{d}V, \tag{1}$$

where T, S, D, E represent the mechanical stress and strain as well as the electrical displacement and field. V is the volume of the piezoelement. A one-dimensional strain distribution within the piezoelement in axis direction i is assumed. According to [6] the axis of polarization is defined as x_3. Therefore the transversal effect is represented by $i = 1$, where the mechanical strain is normal to the direction of polarization, and the longitudinal effect by $i = 3$, where the mechanical strain is in the direction of polarization. After some mathematical calculations, see [9] the energy can be written as

$$U = \frac{1}{2} \frac{Q_\mathrm{p}^2}{C_\mathrm{p}} + \frac{1}{2} \frac{1}{s_{ii}^\mathrm{E}} \int_V \left[S_i^2 + \frac{k_{3i}^2}{1 - k_{3i}^2} \Delta S_{i,3}^2 \right] \mathrm{d}V + \frac{1}{2} \frac{\alpha^2}{C_\mathrm{p}} \left(\ell_i \bar{S}_i \right)^2 - \frac{1}{2} 2 \frac{\alpha}{C_\mathrm{p}} \ell_i \bar{S}_i Q_\mathrm{p}. \tag{2}$$

The electrical charge at the electrodes is termed Q_p, while the mechanical compliance in axis direction i is given as s_{ii}. Further on, the material coupling of the piezoelement is given by $k_{3i} = d_{3i}^2 / \left(s_{ii}^\mathrm{E} \varepsilon_{33}^\mathrm{T} \right)$. In the following, the stiffness c_p in x_i direction, the capacitance C_p of the piezoceramics and the piezoelectric force factor α are introduced as

$$\begin{aligned} c_\mathrm{p} &= \frac{1}{s_{ii}^\mathrm{E}} \frac{V}{\ell_i^2}, \\ C_\mathrm{p} &= \varepsilon_{33}^\mathrm{T} \left(1 - k_{3i}^2 \right) \frac{A_\mathrm{el}}{\ell_3}, \\ \alpha &= \frac{d_{3i}}{s_{ii}^\mathrm{E}} \frac{A_\mathrm{el}}{\ell_i}. \end{aligned} \tag{3}$$

They depend on the area of electrodes A_el, the piezoelectric constant d_{3i}, the permittivity ε_{33} as well as the geometry of the piezoelement (length ℓ_3 between electrodes and length ℓ_i of the piezoelement in direction of mechanical strain).

The energy terms in Equation 2 can be classified as the stored electrical energy, the stored mechanical energy and the converted energy. For convenience of the following calculations,

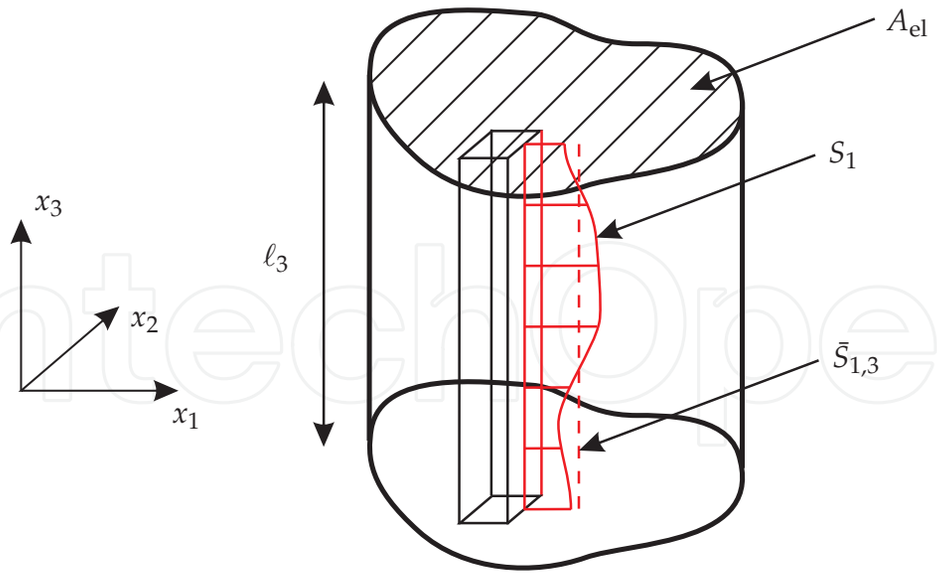

Figure 1. Piezoelement with uniaxial strain distribution.

the mechanical strain is split into the mean value $\bar{S}_i$, the mean strain $\bar{S}_{i,3}$ along the x_3 axis (between the electrodes), and the difference $\Delta S_{i,3}$ between the actual strain and $\bar{S}_{i,3}$,

$$\bar{S}_{i,3}(x_1, x_2) = \frac{\int_0^{\ell_3} S_i(x_1, x_2, x_3)\mathrm{d}x_3}{\ell_3}, \quad \Delta S_{i,3} = S_i - \bar{S}_{i,3}. \tag{4}$$

The reason for this representation is that piezoelectric systems with a homogeneous strain distribution is readliy described by $\Delta S_{i,3} = 0$, which strongly simplifies the calculations. Additionally, the influence of an uneven strain distribution can be seen in the term $\Delta S_{i,3}$. See Figure 1 for an illustration of these definitions.

In case of a continuous system it is reasonable to discretize it for the further analysis. The mechanical deformation is then described by n degrees of freedom (DOF) q_i, while the charge Q_{p} is the electrical DOF,

$$\mathbf{q} = \begin{bmatrix} \mathbf{q}_{\mathrm{mech}} \\ Q_{\mathrm{p}} \end{bmatrix}. \tag{5}$$

Each mechanical DOF is associated with a global mode shape, which defines the mechanical strain distribution S_i within the piezoelectric volume (and the rest of the mechanical system). The overall strain distribution is then the sum of all mode shapes. In order to rewrite the energy term in Equation 2, the term $-\ell_i \bar{S}_i$, which represents the mean deformation of the piezoelement in x_i direction, will be represented by

$$-\ell_i \bar{S}_i = \sum_{k=1}^{n} \kappa_k q_k. \tag{6}$$

Here, a mechanical coupling vector $\boldsymbol{\kappa}$ is introduced. In that form, the energy terms in Equation 2 can be rewritten as

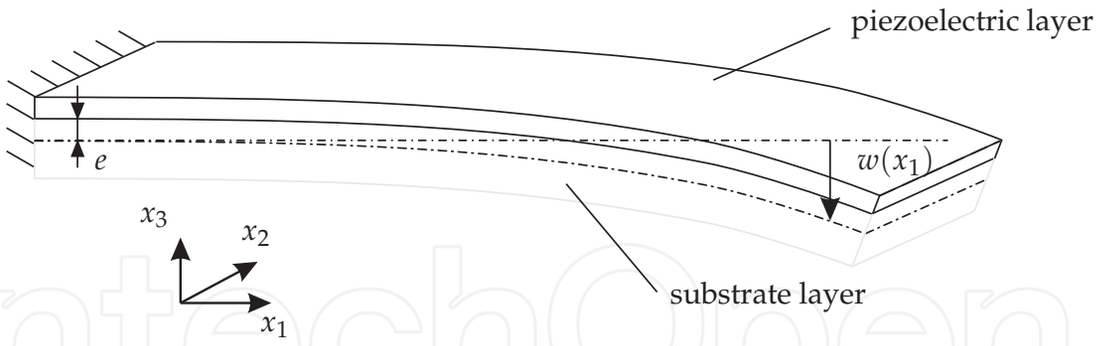

Figure 2. Piezoelectric bimorph.

$$-\frac{1}{2}2\frac{\alpha}{C_\mathrm{p}}\ell_i\bar{S}_iQ_\mathrm{p} = \frac{1}{2}\mathbf{q}^\mathrm{T}\begin{bmatrix}\mathbf{0} & \frac{\alpha}{C_\mathrm{p}}\boldsymbol{\kappa}\\ \frac{\alpha}{C_\mathrm{p}}\boldsymbol{\kappa}^\mathrm{T} & 0\end{bmatrix}\mathbf{q}$$

$$\frac{1}{2}\frac{\alpha^2}{C_\mathrm{p}}\left(\ell_i\bar{S}_i\right)^2 = \frac{1}{2}\mathbf{q}^\mathrm{T}\begin{bmatrix}\frac{\alpha^2}{C_\mathrm{p}}\boldsymbol{\kappa}\boldsymbol{\kappa}^\mathrm{T} & \mathbf{0}\\ \mathbf{0} & 0\end{bmatrix}\mathbf{q}$$

$$\frac{1}{2}\frac{1}{s_{ii}^\mathrm{E}}\int_V\left[S_i^2+\frac{k_{3i}^2}{1-k_{3i}^2}\Delta S_{i,3}^2\right]\mathrm{d}V = \frac{1}{2}\mathbf{q}^\mathrm{T}\begin{bmatrix}C_\mathrm{mech} & \mathbf{0}\\ \mathbf{0} & 0\end{bmatrix}\mathbf{q}. \tag{7}$$

The potential energy can be rewritten as

$$U = \frac{1}{2}\mathbf{q}^\mathrm{T}\mathbf{C}\mathbf{q}, \tag{8}$$

so that the stiffness matrix of the system follows as

$$\mathbf{C} = \begin{bmatrix}\mathbf{C}_\mathrm{mech}+\frac{\alpha^2}{C_\mathrm{p}}\boldsymbol{\kappa}\boldsymbol{\kappa}^\mathrm{T} & \frac{\alpha}{C_\mathrm{p}}\boldsymbol{\kappa}\\ \frac{\alpha}{C_\mathrm{p}}\boldsymbol{\kappa}^\mathrm{T} & \frac{1}{C_\mathrm{p}}\end{bmatrix}. \tag{9}$$

The term $\mathbf{C}_\mathrm{mech}$ represents the 'mechanical' stiffness matrix of the piezoelement, which can be deduced in the same way as standard mechanical systems.

2.2. Piezoelectric bimorph

Now we can apply the above obtained results for the piezoelectric bimorph. We are considering the general case of a piezoelectric layer which has a distance e to the neutral axis of the beam. The coordinate axes are defined in such a way that the origin is at contact between the piezoelectric and the substrate layers at the clamped end, see Figure 2. The x_1 axis is in beam direction and the deformations occur in x_3 direction, which is also the direction of polaziration. With Euler-Bernoulli assumptions the strain is only applied in x_1 direction. That means the transversal effect of the piezoceramics is utilized. The strain terms described in the

previous section then read for the case of the clamped beam:

$$\bar{S}_{1,3} = \frac{\int_0^{\ell_3} S_1 \mathrm{d}x_3}{\ell_3} = -\left(e + \frac{\ell_3}{2}\right) w''(x_1,t),$$

$$\Delta S_{1,3} = S_1 - \bar{S}_{1,3} = \left(\frac{\ell_3}{2} - x_3\right) w''(x_1,t),$$

$$\bar{S}_1 = -\left(e + \frac{\ell_3}{2}\right) \frac{\int_0^{\ell_1} w''(x_1,t)\mathrm{d}x_1}{\ell_1} = -\left(e + \frac{\ell_3}{2}\right) \frac{w'(\ell_1) - w'(0)}{\ell_1}. \tag{10}$$

The bending of the beam is described by $w(x_1,t)$. This term will be split into the part depending on coordinate x_1 and the part depending on time t,

$$w(x_1,t) = W(x_1)q(t), \quad w''(x_1,t) = W''(x_1)q(t). \tag{11}$$

In this example, only one mechanical degree of freedom is used to describe the vibrations. This is typically a reasonable approximation when the system vibrates close to one of its eigenfrequencies. In this way, the general stiffness matrix according to Equation 9 reduces to

$$\mathbf{C} = \begin{bmatrix} c_{\mathrm{mech}} + \frac{\alpha^2}{C_\mathrm{p}}\kappa^2 & \frac{\alpha}{C_\mathrm{p}}\kappa \\ \frac{\alpha}{C_\mathrm{p}}\kappa & \frac{1}{C_\mathrm{p}} \end{bmatrix}, \tag{12}$$

and the mechanical coupling is written as

$$\kappa = \left(e + \frac{\ell_3}{2}\right)\left(W'(\ell_1) - W'(0)\right), \tag{13}$$

while the piezoelectric coupling reads

$$\frac{\alpha}{C_\mathrm{p}} = \frac{k_{31}^2}{1-k_{31}^2}\frac{1}{d_{31}}\frac{\ell_3}{\ell_1}, \quad \frac{\alpha^2}{C_\mathrm{p}} = \frac{1}{s_{11}^\mathrm{E}}\frac{k_{31}^2}{1-k_{31}^2}\frac{\ell_2\ell_3}{\ell_1}. \tag{14}$$

Terms of the kind $\frac{\alpha^2}{C_\mathrm{p}}\kappa^2$, which determine the increase in eigenfrequencies between short circuit electrodes and isolated electrodes are obtained as

$$\frac{\alpha^2}{C_\mathrm{p}}\kappa^2 = \frac{1}{s_{11}^\mathrm{E}}\frac{k_{31}^2}{1-k_{31}^2}\frac{\ell_2\ell_3}{\ell_1}\left(e + \frac{\ell_3}{2}\right)^2\left(W'(\ell_1) - W'(0)\right)^2. \tag{15}$$

For a better understanding of these terms, it is useful to introduce the area moment of inertia I^{PZT} of the piezoceramics around its own center of gravity and the moment of inertia I^{nF} around the neutral axis of the beam. Additionally, also the difference $I^{\mathrm{nF}} - I^{\mathrm{PZT}}$ is included

in the results,

$$I^{\mathrm{PZT}} = \frac{\ell_2 \ell_3^3}{12},$$

$$I^{\mathrm{nF}} = \frac{\ell_2 \ell_3^3}{12} + \left(e + \frac{\ell_3}{2}\right)^2 \ell_2 \ell_3,$$

$$I^{\mathrm{nF}} - I^{\mathrm{PZT}} = \left(e + \frac{\ell_3}{2}\right)^2 \ell_2 \ell_3. \tag{16}$$

With these definitions, the coupling terms can be expressed as

$$\frac{\alpha^2}{C_{\mathrm{p}}}\kappa^2 = \frac{1}{s_{11}^{\mathrm{E}}} \frac{k_{31}^2}{1-k_{31}^2} \frac{I^{\mathrm{nF}} - I^{\mathrm{PZT}}}{\ell_1} \left(W'(\ell_1) - W'(0)\right)^2. \tag{17}$$

This result can be used to discuss different geometries and types of bimorphs. Obviously a beam that consists only of piezoelectric material does not have any coupling at all, because the distance e is exactly one half of the thickness of the piezoelectric layer, $e = -\frac{\ell_3}{2}$. This means the term $I^{\mathrm{nF}} - I^{\mathrm{PZT}}$ vanishes. Contrary to this, a beam which is made of two identical piezoelectric layer is represented by $e = 0$ because of the symmetry, and a coupling exists. However, yet more efficient is the design of bimorphs or trimorphs with a substrate layer, which moves the neutral axis away from the surface of the piezoelectric layer. This results in a positive value $e > 0$. The best type is a symmetric trimorph with identical piezoelectric layers on both sides of the substrate layer. Here the distance equals half of the substrate layer. More details about the optimization of bimorphs can be found in [10].

In general, the piezomechanical system can be described by the following differential equations,

$$\begin{bmatrix} m_{\mathrm{mech}} & 0 \\ 0 & 0 \end{bmatrix} \begin{bmatrix} \ddot{q} \\ \ddot{Q}_{\mathrm{p}} \end{bmatrix} + \begin{bmatrix} c_{\mathrm{mech}} + \frac{\alpha^2}{C_{\mathrm{p}}}\kappa^2 & \frac{\alpha}{C_{\mathrm{p}}}\kappa \\ \frac{\alpha}{C_{\mathrm{p}}}\kappa & \frac{1}{C_{\mathrm{p}}} \end{bmatrix} \begin{bmatrix} q \\ Q_{\mathrm{p}} \end{bmatrix} = \begin{bmatrix} F(t) \\ -u_{\mathrm{p}}(t) \end{bmatrix}, \tag{18}$$

with the modal mass m_{mech}, the external force $F(t)$ and the voltage $u_{\mathrm{p}}(t)$ at the electrodes of the piezoelement.

2.3. Linear energy harvester

Based on these results, the simplest and linear energy harvester can be modeled. In this case only a resistor is connected as an electrical load at the electrodes of the piezoelement. Therefore the voltage u_{p} is dependent on the time derivative of charge $\dot{Q}_{\mathrm{p}}$ and the differential equations of motions for this case including damping d_{mech} read

$$\begin{bmatrix} m_{\mathrm{mech}} & 0 \\ 0 & 0 \end{bmatrix} \begin{bmatrix} \ddot{q} \\ \ddot{Q}_{\mathrm{p}} \end{bmatrix} + \begin{bmatrix} d_{\mathrm{mech}} & 0 \\ 0 & R \end{bmatrix} \begin{bmatrix} \dot{q} \\ \dot{Q}_{\mathrm{p}} \end{bmatrix} + \begin{bmatrix} c_{\mathrm{mech}} + \frac{\alpha^2}{C_{\mathrm{p}}}\kappa^2 & \frac{\alpha}{C_{\mathrm{p}}}\kappa \\ \frac{\alpha}{C_{\mathrm{p}}}\kappa & \frac{1}{C_{\mathrm{p}}} \end{bmatrix} \begin{bmatrix} q \\ Q_{\mathrm{p}} \end{bmatrix} = \begin{bmatrix} F(t) \\ 0 \end{bmatrix} \tag{19}$$

We seek for the amplitudes of the stationary oscillations,

$$\hat{\mathbf{q}} = \left(-\Omega^2\mathbf{M} + j\Omega\mathbf{D} + \mathbf{C}\right)^{-1} \begin{bmatrix} \hat{F} \\ 0 \end{bmatrix}, \tag{20}$$

with the corresponding system matrices according to Equation 19. The amplitudes of the time signals are marked by a hat. With the stationary charge amplitude $\hat{Q}_\mathrm{p}$ the instantaneous power $p(t)$ can be calculated,

$$p(t) = Ri_\mathrm{p}^2(t) = R\Omega^2\hat{Q}_\mathrm{p}^2\cos^2(\Omega t), \tag{21}$$

where i_p is the current. The energy that is dissipated in the resistor will be treated as the stationary harvested energy $E_\mathrm{h,stat}$. It is then the integral of the power p,

$$E_\mathrm{h,stat} = \int_0^{\frac{2\pi}{\Omega}} p(t)\mathrm{d}t = \pi R\Omega\hat{Q}_\mathrm{p}^2. \tag{22}$$

This result, normalized to force amplitude, is shown in Figure 3 versus the load resistance R and the excitation frequency Ω, normalized to the mechanical eigenfrequenzcy ω_0. For this study, the following system parameters are used:

$$\begin{aligned} m_\mathrm{mech} &= 0.005\mathrm{kg}, \\ d_\mathrm{mech} &= 0.1212\mathrm{Ns/m}, \\ c_\mathrm{mech} &= 341.2651\mathrm{N/m}, \\ \alpha\kappa &= 0.002, \\ C_\mathrm{p} &= 83.676\mathrm{nF}. \end{aligned} \tag{23}$$

Obviously the harvested energy is highly frequency dependent. Only in a narrow frequency range around the eigenfrequency the efficiency is high. Also the resistor must be tuned for maximum harvested energy. The system is less sensitive towards changes of the resistance, but one can show that the optimal resistance which is optimal for low coupling and/or high damping is obtained as

$$R_\mathrm{opt} = \frac{1}{\Omega C_\mathrm{p}} \tag{24}$$

3. Array configuration

Utilizing an array configuration for the extension of the generator bandwidth is a commonly used approach. The idea is simple and powerfull: multiple generator elements are tuned to slightly (a few %) different eigenfrequencies. A major factor is the connection to the electrical system; if each individual element uses its own bridge rectifier, the elements are electrically uncoupled and their output power simply can be summed up. However, individual bridge

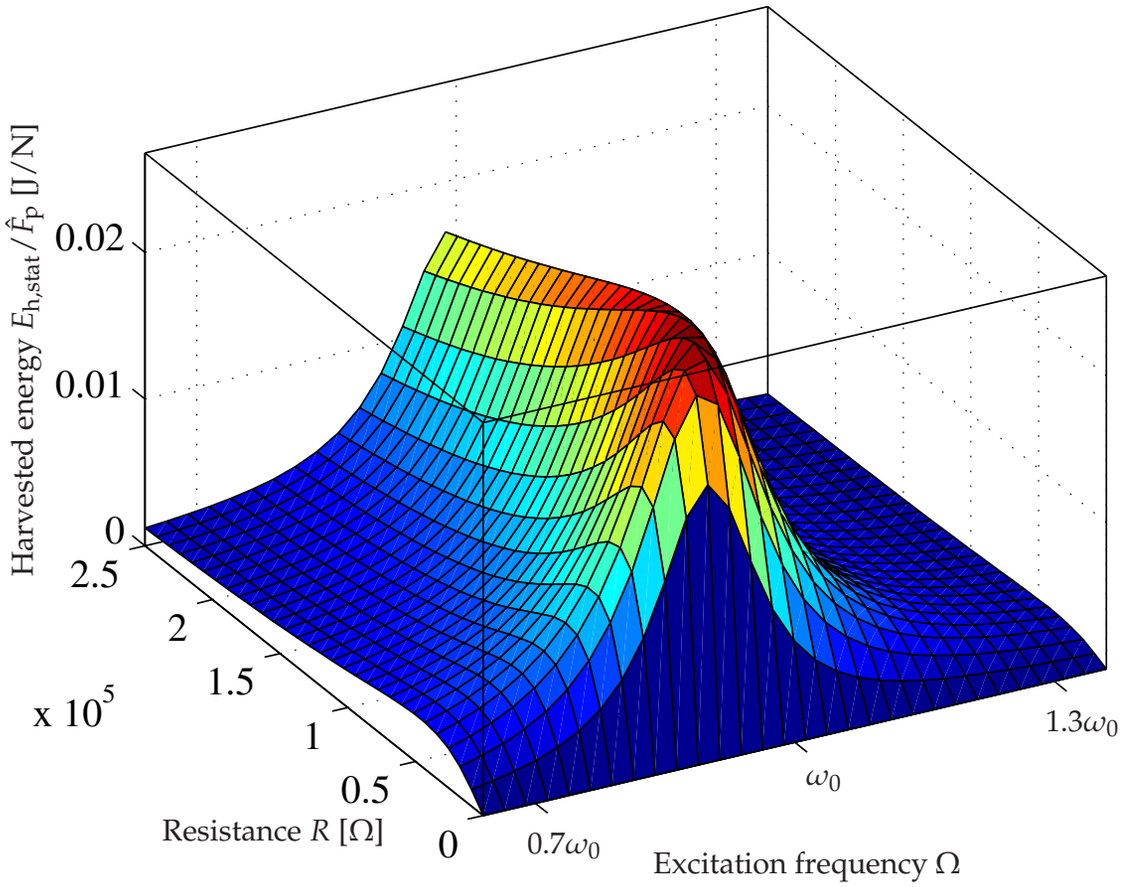

Figure 3. Harvested energy $E_{h,stat}$ versus normalized excitation frequency Ω and load resistance R.

rectifiers are a comparable big effort, a huge number of elements and cables is needed, further the voltage drop over each diode is also summed up, so that the losses increase. As soon the individual elements are made of one part the electrodes are connected naturally, which results automatically in parallel connected elements. In such a configuration, Figure 4, the elements are electrically coupled.

This section investigates the effect of the electrical coupling on the performance of piezoelectric energy harvesting generators. Two configurations are investigated, the electrical parallel connection as well as the electrical serial connection. Both cases are utilizing two elements as most basic version of a piezoelectric array. The model is based on the linear generator model in Equation 19, therefore a fore excitation is assumed. We further assume that the applied fore is equal on all elements, representing a common support. The resonance frequency tuning is made by an adoption of the modal mass of the elements (change of tip mass), all other parameters are assumed to be constant. The configurations including boundary conditions is given in Figure 4. Each element can be represented by the linear Equation 19. In the parallel configuration the two voltages are equal and $u_{P_1} = u_{P_2} =$

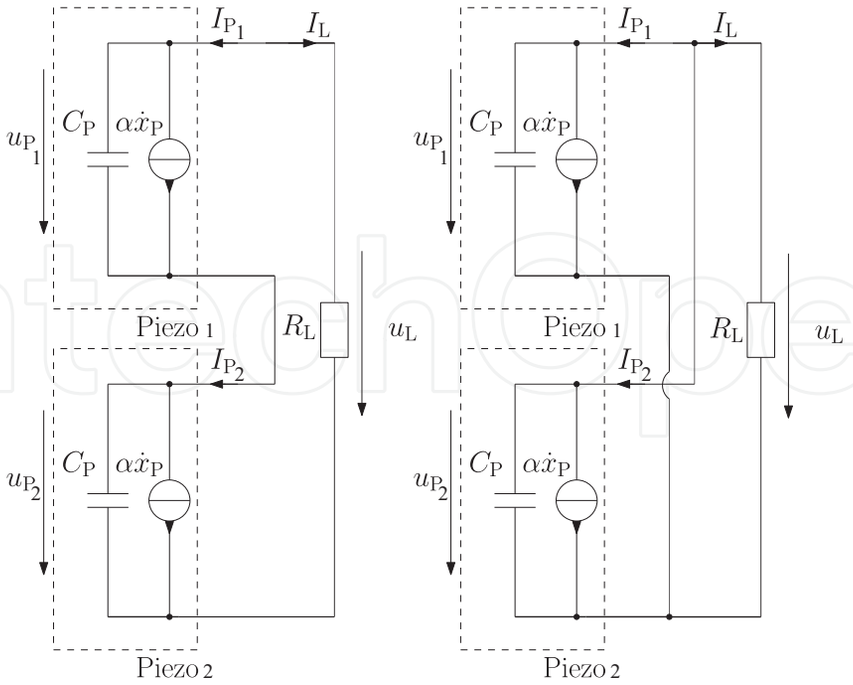

Figure 4. Schematic Circuit. Left: series configuration. Right: parallel configuration

$R_L\,(i_{P_1} + i_{P_2})$ apply due to Kirchhoff's rules. Using both, the parallel configuration is described by

$$\begin{bmatrix} m_{\text{mech}} - \Delta m & 0 & 0 & 0 \\ 0 & m_{\text{mech}} + \Delta m & 0 & 0 \\ 0 & 0 & 0 & 0 \\ 0 & 0 & 0 & 0 \end{bmatrix} \begin{bmatrix} \ddot{q}_1 \\ \ddot{q}_2 \\ \ddot{Q}_{p1} \\ \ddot{Q}_{p2} \end{bmatrix} + \begin{bmatrix} d_{\text{mech}} & 0 & 0 & 0 \\ 0 & d_{\text{mech}} & 0 & 0 \\ 0 & 0 & R & R \\ 0 & 0 & R & R \end{bmatrix} \begin{bmatrix} \dot{q}_1 \\ \dot{q}_2 \\ \dot{Q}_{p1} \\ \dot{Q}_{p2} \end{bmatrix}$$

$$\ldots + \begin{bmatrix} c_{\text{mech}} + \frac{\alpha^2}{C_p}\kappa^2 & 0 & \frac{\alpha}{C_p}\kappa & 0 \\ 0 & c_{\text{mech}} + \frac{\alpha^2}{C_p}\kappa^2 & 0 & \frac{\alpha}{C_p}\kappa \\ \frac{\alpha}{C_p}\kappa & 0 & \frac{1}{C_p} & 0 \\ 0 & \frac{\alpha}{C_p}\kappa & 0 & \frac{1}{C_p} \end{bmatrix} \begin{bmatrix} q_1 \\ q_2 \\ Q_{p1} \\ Q_{p2} \end{bmatrix} = \begin{bmatrix} F(t) \\ F(t) \\ 0 \\ 0 \end{bmatrix}. \tag{25}$$

The coupling between the elements is obviously seen in the damping matrix. In the series configuration, the current at both generators is equal. Therefore $u_{P_1} + u_{P_2} = R_L i_{P_1} = R_L i_{P_2}$ is applied to couple the two generators:

$$\begin{bmatrix} m_{\text{mech}} - \Delta m & 0 & 0 \\ 0 & m_{\text{mech}} + \Delta m & 0 \\ 0 & 0 & 0 \end{bmatrix} \begin{bmatrix} \ddot{q}_1 \\ \ddot{q}_2 \\ \ddot{Q}_p \end{bmatrix} + \begin{bmatrix} d_{\text{mech}} & 0 & 0 \\ 0 & d_{\text{mech}} & 0 \\ 0 & 0 & R \end{bmatrix} \begin{bmatrix} \dot{q}_1 \\ \dot{q}_2 \\ \dot{Q}_p \end{bmatrix} + \ldots$$

$$\begin{bmatrix} c_{\text{mech}} + \frac{\alpha^2}{C_p}\kappa^2 & 0 & \frac{\alpha}{C_p}\kappa \\ 0 & c_{\text{mech}} + \frac{\alpha^2}{C_p}\kappa^2 & \frac{\alpha}{C_p}\kappa \\ \frac{\alpha}{C_p}\kappa & \frac{\alpha}{C_p}\kappa & \frac{2}{C_p} \end{bmatrix} \begin{bmatrix} q_1 \\ q_2 \\ Q_p \end{bmatrix} = \begin{bmatrix} F(t) \\ F(t) \\ 0 \end{bmatrix}. \tag{26}$$

Here the coupling is evidently in the stiffness matrix. Where all parameters correspond to the ones from the modeling section. The mass for frequency adoption is $\Delta m = 0.5g$. For the steady state the system can be solved and the transfer functions can be determined analog to the single system. The total dissipated energy at the resistor is again given by

$$E_{\mathrm{h,stat}} = \int_0^{\frac{2\pi}{\Omega}} u(t)i(t)\mathrm{d}t. \tag{27}$$

Evaluating this equation for voltage and current over the load resistor gives the gained energy for the application, the result is depicted in Figure 5 for serial configuration and in Figure 6 for parallel configuration. For the in series connected generators the bandwidth is widened at high impedance loads and it is not significantly changed for low impedances. For the parallel configuration, a bandwidth expanded at low impedance loads and also not changed for high impedances.

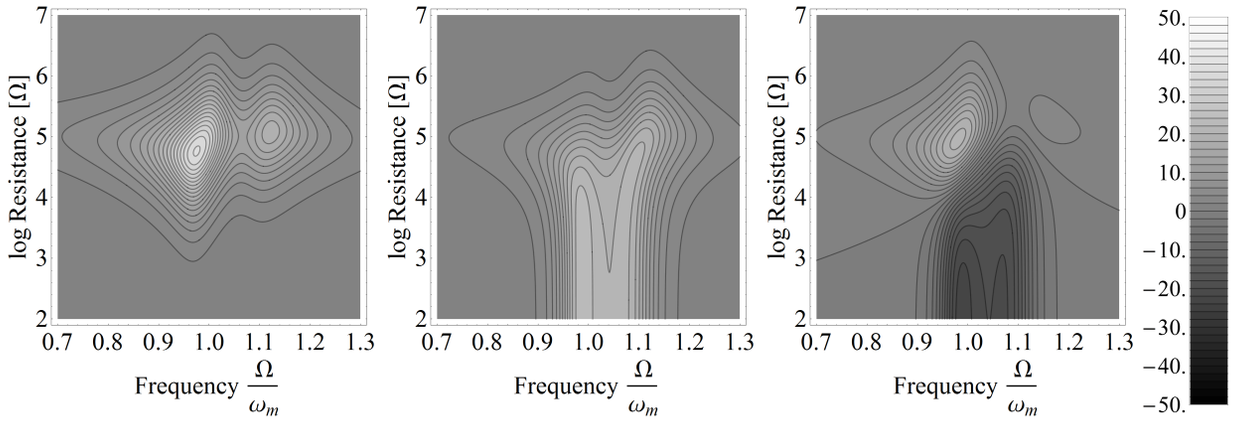

Figure 5. Energy per period in serial configuration in mJ/N. Left: gained useable energy. Middle: element 1. Right: element2.

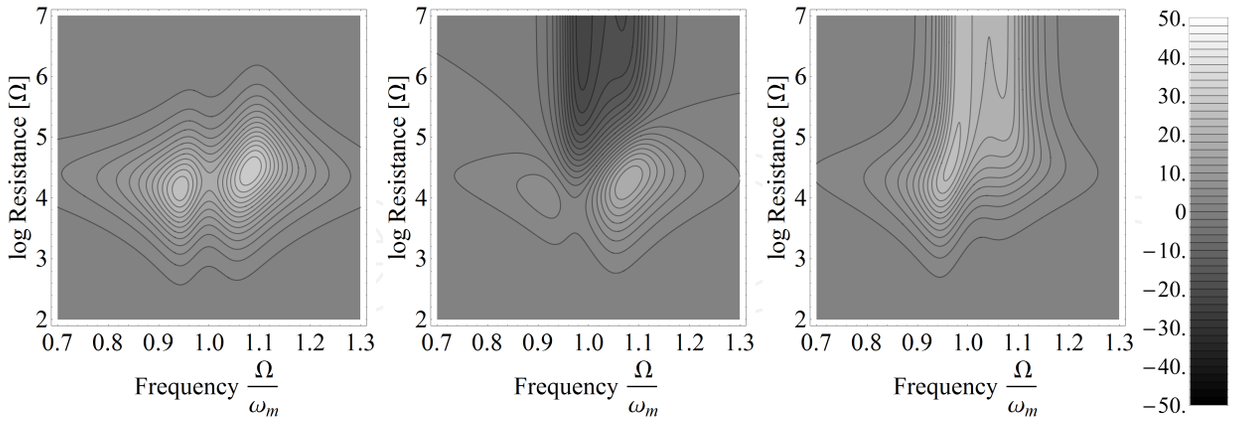

Figure 6. Energy per period in parallel configuration in mJ/N. Left: gained useable energy. Middle: element 1. Right: element2.

To explain why there is no widening of the bandwidth in serial connection at low impedances the Equation 27 is evaluated for both elements, using the individual voltage and the common current. Figure 5 show that the second element works as energy sink for low impedances, with the consequence, that the energy generated by element one is used to actuate the other one. Figure 7 shows this effect. Even with the overall maximum displacement of element two

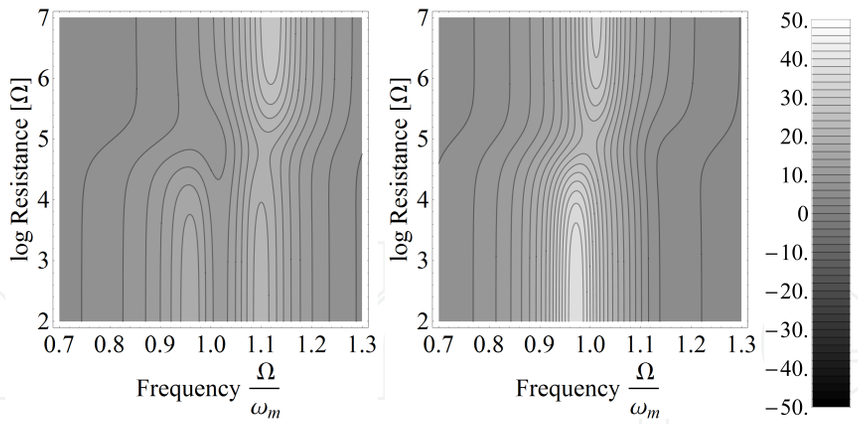

Figure 7. Tip displacement of both elements in serial configuration in mm/N. Left: element 1. Right: element2.

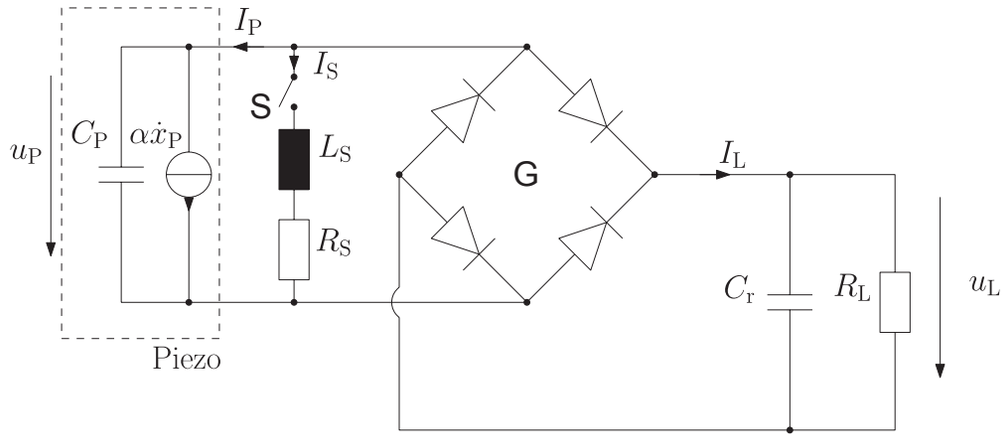

Figure 8. Schematic of SSHI circuit.

at low impedances the gained useable energy is low. The same effect but for high impedances is shown in Fig. 6 for the parallel configuration. In this case element one is the energy sink.

Concluding, the utilization of arrays with serials or parallel electrical coupling has only a major positiv effect on the bandwidth for a matched impedance, for unmatched impedances the coupling can be a drawback. The bandwidth can be enlarged with any further element, the mean energy output over bandwidth in general is higher if the mistuning of the resonance frequencies is smaller. For power and bandwidth comparison of generator arrays it is reasonable to keep the volume of active material constant.

4. Switching networks (SSHI)

An important technique to enhance the energy extraction is to use nonlinear switching networks. In detail, the 'Synchronized Switch Harvesting on Inductor' (SSHI) technique is studied. Such networks are an active field of research [3, 4, 7]. The corresponding network is shown in Figure 8. This nonlinear electric circuit consists of a switching LR-branch, a rectifier and load capacitor C_r. The load is again described as a resistor R_L. Assuming a sinusoidal mechanical deformation of the piezoceramics, the switch is briefly closed on minima and maxima of the deformation. During these times, an oscillating electric circuit is formed, as the capacitive piezoelectric transducer and the inductance are connected. During this electrical

semi-period the switch is kept close and the voltage is inverted. As this electrical period time is generally much shorter than the mechanical one, this occurs nearly instantaneously. After inversion, the switch is opened again until the next deformation extremum. Consequently, the resulting voltage signal at the piezoelectrodes is nearly rectangular-shaped. Previous publications have proven the enhanced performance of SSHI circuits especially for systems with low piezoelectrical coupling.

The modeling and optimization of such networks is not straight forward, as the overall system is nonlinear. In the following we will present a modeling technique that is based on the harmonic balance method.

4.1. Period response for harmonic excitation

Firstly, the periodic response if the SSHI is studied. In order to simplify the results, the following approximations are defined,

$$L_\mathrm{s} \to 0, \quad C_\mathrm{r} \to \infty. \tag{28}$$

and the electrical losses remain constant. In practical realizations, all approximations are appropriate. A small inductance value results in a fast inversion, and a large storage capacitor means that the voltage at the load is nearly constant. Both situations are typically wanted. Further on, the nonlinear system can be treated as a piecewise linear system.

In order to obtain the stationary voltage signal it is necessary to study one semi-period of the system and consider the stationarity condition, which means the signal repeats after each period. We define the time axis in such a way that for $t = 0$ the voltage was just inverted and the switch is opened. With the approximation $C_\mathrm{r} \to \infty$ the voltage u_L at the load capacitor is constant at u_0. This value has to be calculated yet. Because of the loss resistances - described by the electrical damping ratio ζ - the voltage changes from $\pm u_0$ to $\mp u_0 \mathrm{e}^{-\pi\zeta}$. That means the absolute value of the voltage u_p at the piezoelectrodes after inversion is smaller than the voltage at the load u_0. Therefore the recifier blocks, and the piezovoltage changes linearly with the piezodeformation q,

$$u_\mathrm{p}(t) = -\frac{\alpha\kappa}{C_\mathrm{p}} q(t) + C_0, \tag{29}$$

with an integration constant C_0. According to the definitions, the piezodeformation must have an extremum at $t = 0$, so that the time signal reads

$$q(t) = \hat{q} \cos(\Omega t), \tag{30}$$

and for the voltage signal it follows

$$u_\mathrm{p}(t) = -\frac{\alpha\kappa}{C_\mathrm{p}} \hat{q} \cos(\Omega t) + u_0 \mathrm{e}^{-\pi\zeta} + \frac{\alpha\kappa}{C_\mathrm{p}} \hat{q}. \tag{31}$$

The voltage amplitude u_0 is still unknown, but at least the time t_1 can be calculated, at which the voltage at the piezoelectrodes equals the voltage at the load, $u_\mathrm{p}(t = t_1) = u_0$:

$$t_1 = \operatorname{acos}\left[\frac{u_0}{\frac{\alpha\kappa}{C_\mathrm{p}} \hat{q}} \left(\mathrm{e}^{-\pi\zeta} - 1 \right) + 1 \right] / \Omega. \tag{32}$$

At this time t_1 the rectifier changes from 'blocking' to 'conducting'. Practically this means that the piezovoltage remains constant at u_0 from t_1 until the end of the semi-period $T/2$.

The piezovoltage u_0 can be calculated based on the energy balance. Therefore, the transferred energy E_t, the harvested energy E_h and the energy dissipated in the switching branch E_s must be obtained. They read, respectively,

$$\begin{aligned}
E_\mathrm{t} &= -2\int_0^{T/2} F_\mathrm{p}(t)\dot{q}(t)\mathrm{d}t = 2\alpha\kappa\Omega\hat{q}\left[\int_0^{t_1} u_\mathrm{p}(t)\sin(\Omega t)\,\mathrm{d}t + \int_{t_1}^{T/2} u_0\sin(\Omega t)\,\mathrm{d}t\right],\\
E_\mathrm{h} &= 2\int_0^{T/2}\frac{u_0^2}{R}\mathrm{d}t = 2\frac{\pi}{\Omega}\frac{u_0^2}{R},\\
E_\mathrm{s} &= 2\frac{1}{2}C_\mathrm{p}u_0^2\left[1-\left(\mathrm{e}^{-\pi\zeta}\right)^2\right].
\end{aligned} \tag{33}$$

The transferred energy corresponds to the total energy that is shifted from the mechanical system into the piezoelectric system, while the other terms are the energies that are dissipated within the load resistor and the resistor of the switching branch. In stationary situation, the equality

$$E_\mathrm{t} = E_\mathrm{h} + E_\mathrm{s} \tag{34}$$

holds. With this equation, finally the stationary voltage amplitude can be recalculated as

$$u_0 = 2\frac{\alpha\kappa}{C_\mathrm{p}\left(1-\mathrm{e}^{-\pi\zeta}\right)+\frac{\pi}{\Omega R}}\hat{q}. \tag{35}$$

Figure 9 shows the time signal of the voltage u_p. Inserting the stationary voltage amplitude into the energies in Equation 33 gives us the stationary energies,

$$\begin{aligned}
E_\mathrm{t,stat} &= 4\frac{\alpha^2\kappa^2}{C_\mathrm{p}}\frac{1-\mathrm{e}^{-2\pi\zeta}+\frac{2\pi}{C_\mathrm{p}\Omega R}}{\left(1-\mathrm{e}^{-\pi\zeta}+\frac{\pi}{C_\mathrm{p}\Omega R}\right)^2}\hat{q}^2,\\
E_\mathrm{h,stat} &= 4\frac{\alpha^2\kappa^2}{C_\mathrm{p}}\frac{\frac{2\pi}{C_\mathrm{p}\Omega R}}{\left(1-\mathrm{e}^{-\pi\zeta}+\frac{\pi}{C_\mathrm{p}\Omega R}\right)^2}\hat{q}^2,\\
E_\mathrm{s,stat} &= 4\frac{\alpha^2\kappa^2}{C_\mathrm{p}}\frac{1-\mathrm{e}^{-2\pi\zeta}}{\left(1-\mathrm{e}^{-\pi\zeta}+\frac{\pi}{C_\mathrm{p}\Omega R}\right)^2}\hat{q}^2.
\end{aligned} \tag{36}$$

All these energy terms have quadratic dependency with the force factor α, which should be maximized for a high energy conversion. Also the electrical damping ratio ζ in the switching branch should be low. They also grow quadratically with the vibration amplitude $\hat{q}$ of the oscillator.

However, for the force excited vibrations, the vibration amplitude is influenced by the harvesting device. The transferred energy $E_\mathrm{t,stat}$ yields a damping effect upon the oscillator, which reduces the vibration amplitudes. In order to determine the vibration amplitudes,

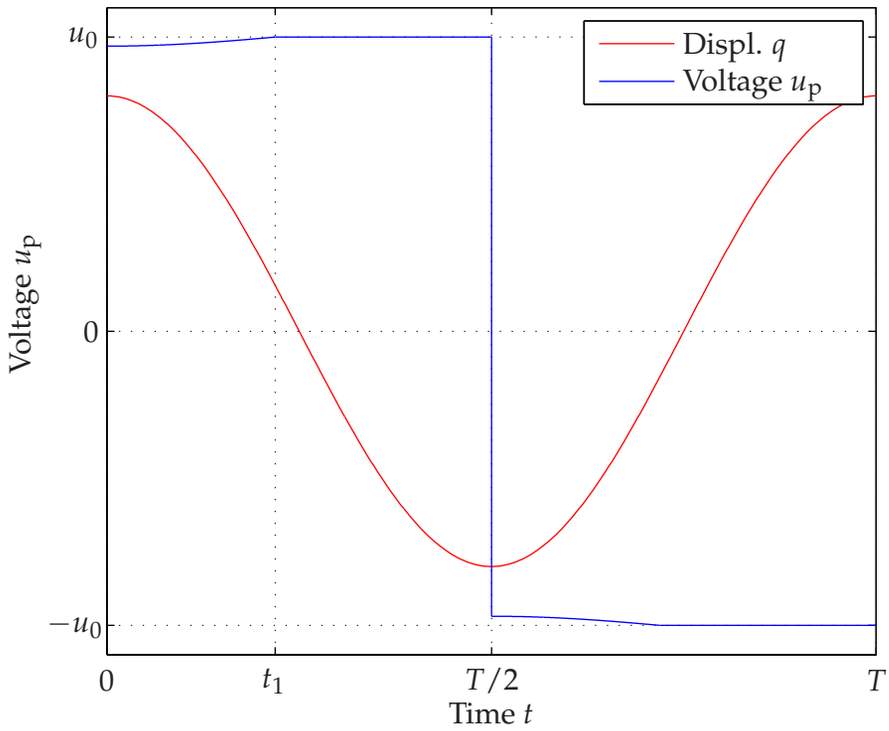

Figure 9. Time signals of piezodeformation and voltage at the electrodes.

the harmonic balance method is applied in the following. In this technique the shunted piezoceramics is replaced by a spring - damper combination. Therefore the period - but not harmonic - force response $F_p(t) = -\alpha u_p(t)$ of the shunted piezoceramics is expressed by its Fourier-series,

$$u_p(t) = \frac{1}{2}a_0 + \sum_{i=1}^{\infty} \left(a_i \cos\left(i\Omega t\right) + b_i \sin\left(i\Omega t\right)\right). \tag{37}$$

The Fourier-coefficients a_i, b_i are obtained by the periodic timesignal $u_p(t)$,

$$a_i = \frac{2}{T}\int_c^{c+T} u_p(t)\cos\left(i\Omega t\right)\mathrm{d}t; \quad b_i = \frac{2}{T}\int_c^{c+T} u_p(t)\sin\left(i\Omega t\right)\mathrm{d}t. \tag{38}$$

The idea of the proposed linearization techniques is to approximate the periodic voltage signal by its main harmonics,

$$u_p(t) \approx a_1 \cos\left(\Omega t\right) + b_1 \sin\left(\Omega t\right). \tag{39}$$

This harmonic force signal is also produced by a spring - damper combination with the following parameters,

$$c^* = \frac{a_1}{\hat{q}}, \quad d^* = -\frac{b_1}{\Omega\hat{q}}. \tag{40}$$

In general, these replacement parameters c^*, d^* are frequency dependent. With these results, the stationary vibration amplitudes of the oscillator with shunted piezoceramics can be recalculated,

$$\hat{q} = \frac{\hat{F}_p}{\left|-m\Omega^2 + j\left(d + d^*\right)\Omega + c + c^*\right|} \tag{41}$$

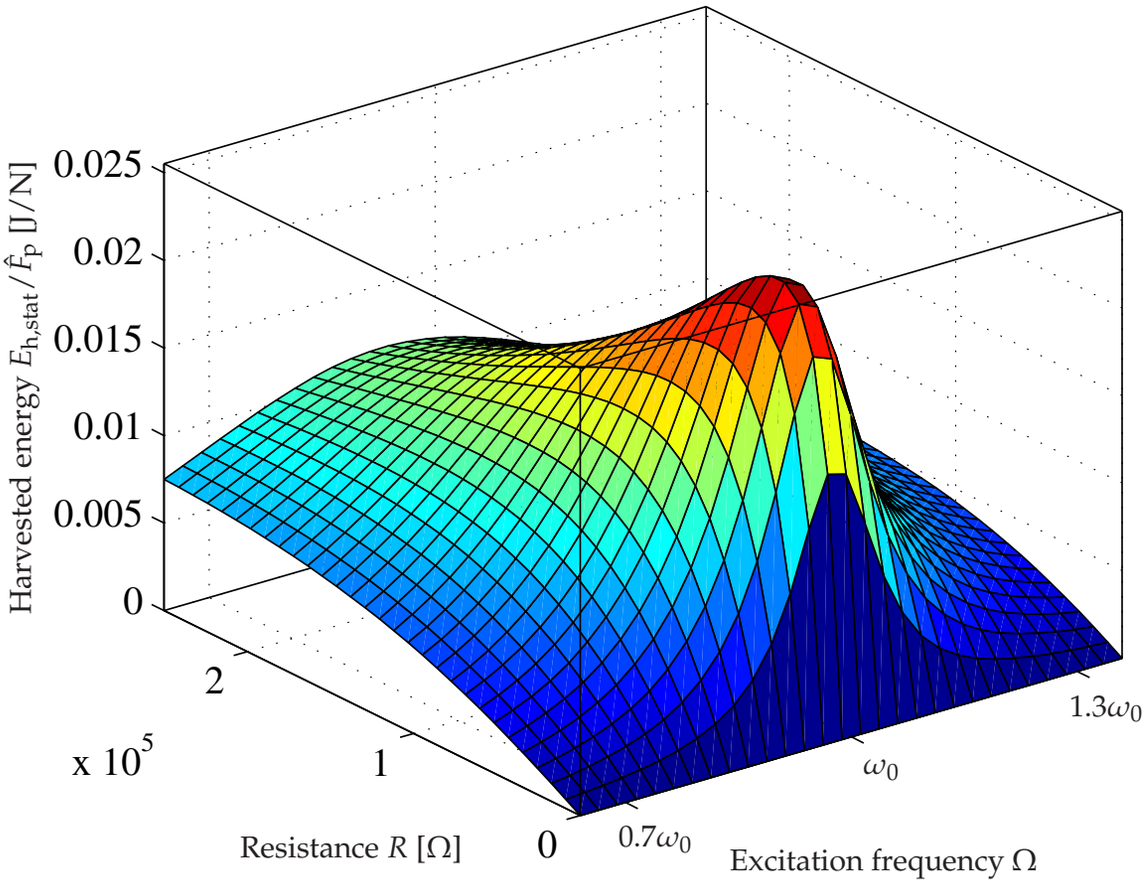

Figure 10. Harvested energy $E_{h,stat}$ versus normalized excitation frequency Ω and load resistance R.

Finally this stationary vibration amplitude $\hat{q}$ can be inserted into Equation 36 for the harvested energy $E_{h,stat}$. The resulting energy is shown in Figure 10 versus the excitation frequency Ω and the load resistance R. This figure can be compared with the linear resistance case in Figure 3. It again shows that most energy is harvested at the resonance frequency ω_0 of the oscillator, because the vibration amplitudes are highest in this case. But also the load resistor must be tuned correctly in order to achieve the maximum energy. Compared to the standard case the maximum amount of harvested energy is similar, while the frequency bandwidth with SSHI tends to be larger. However, the voltage at the load resistance with SSHI circuit is nearly constant which is wanted in most practical cases, while it is a harmonics oscillations with the linear resistance. Additionally the damping effect upon the mechanical structure is higher, because of the additional energy that is dissipated within the resistance of the switching branch.

5. Piezomagnetoelastic energy harvesting

One major drawback for energy harvesting systems is that conventional generators produce the maximum energy when the system is excited at its resonance frequency. If the excitation

frequency shifts the output power is drastically reduced. To overcome this disadvantage multiple researchers work on different broadband techniques to widen the operational frequency range. The focus in this section is on piezomagnetoelastic energy harvesting strategies. The equations of motion (EOM) are derived in the previous section. The generator is based on a model with lumped parameters. The broadband response is achieved by using nonlinear magnetic forces. Piezomagnetoelastic generators are studied in a bunch of multiple research activities [1, 2, 13, 14]. In many approaches the system is modeled as Duffing oscillator. Usually the system parameters in the model are adjusted manually to match the amplitude or power response of the experiment. The aim in this work is to investigate an analytically approach to derive the duffing parameters out of the system parameters.

This section is organized as followed. The mechanical EOM is derived for the piezomagnetoelastic energy harvesting system. In the following the duffing parameters are derived with respect to the system and input parameters and the system dynamic is discussed. The last part shows the analytic solution for large orbit oscillations.

5.1. Modeling of the piezomagnetoelastic energy harvesting system

Figure 11 gives a schematic view of the piezomagnetoelastic system. The energy harvester consist of a cantilever with two piezoelectric patches mounted on each side of an inactive substructure. The system is excited by a harmonic force

$$F(t) = \hat{F}\sin(\omega t) \tag{42}$$

where $\hat{F}$ is the amplitude of the excitation and ω is the excitation frequency. A magnetic tip mass is attached to the free end of the beam. Another permanent magnet is stationary mounted near the free end. The magnets are oppositely poled so they exhibit a repulsive force. The nonlinear magnetic force leads to two stable equilibrium positions. Figure 11 shows both symmetric stable equilibrium positions. The tip displacement is given with q and the magnet spacing is s. The coupled mechanical and electrical differential equations are derived in the previous section

$$m\ddot{q} + d\dot{q} + cq - \frac{\alpha}{C_\mathrm{P}}Q_\mathrm{P} + \frac{dU_\mathrm{mag}}{dq} = F(t) \tag{43}$$

and

$$R\dot{Q}_\mathrm{P} + \frac{1}{C_\mathrm{P}}Q_\mathrm{P} - \frac{\alpha}{C_\mathrm{P}}q = 0. \tag{44}$$

Equation 43 and 44 are similar to 19 where $m = m_\mathrm{mech}$ is the modal mass. The modal damping is d and $c = c_\mathrm{mech} + \frac{\alpha^2}{C_\mathrm{p}}\kappa^2$ is the total mechanical stiffness. Additionally to the linear differential equations the nonlinear magnetic force leads to

$$U_\mathrm{mag} = \frac{\mu_0}{4\pi}\boldsymbol{\nabla}\frac{\boldsymbol{\mu}_\mathrm{A}\mathbf{r}_\mathrm{AB}}{\|\mathbf{r}_\mathrm{AB}\|_2^3}\boldsymbol{\mu}_\mathrm{B} \tag{45}$$

where μ_0 is the permeability of free space, $\boldsymbol{\mu}_A$ and $\boldsymbol{\mu}_B$ are the magnetic dipole moment vectors. $\mathbf{r}_{AB}$ is the vector from the source of magnet B to magnet A. $\|\cdot\|_2$ is the EUKLIDEAN norm and $\boldsymbol{\nabla}$ is the vector gradient defined with

$$\boldsymbol{\nabla}\frac{1}{r^n} = \begin{bmatrix}\partial/\partial x\\ \partial/\partial y\\ \partial/\partial z\end{bmatrix}\frac{1}{r^n} = -\frac{n}{r^{n+1}}\begin{bmatrix}x/r\\ y/r\\ z/r\end{bmatrix} = -\frac{n\mathbf{r}}{r^{n+2}}. \tag{46}$$

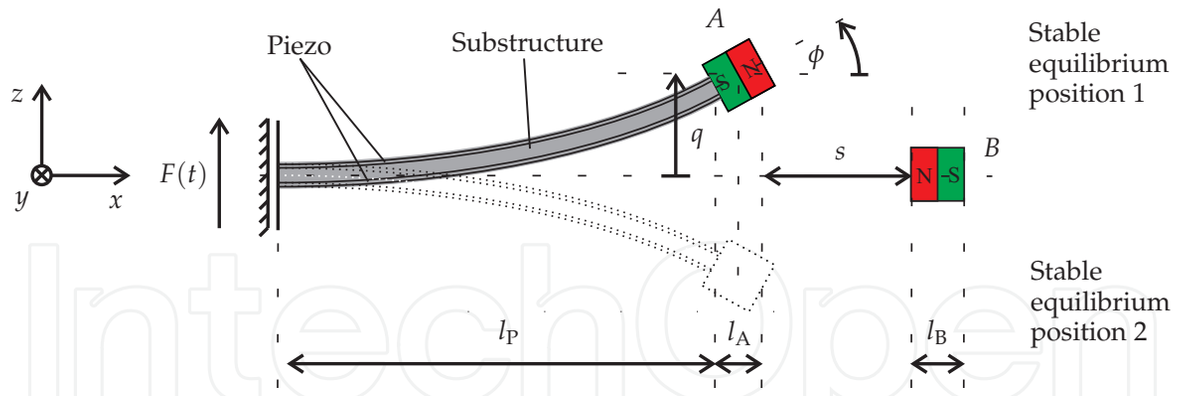

Figure 11. Schematic view of the piezomagnetoelastic energy harvesting system

The magnetic dipole moment vectors are written as

$$\boldsymbol{\mu}_A = M_\mathrm{A} V_\mathrm{A} \begin{bmatrix} \cos\phi \\ 0 \\ \sin\phi \end{bmatrix}, \tag{47a}$$

$$\boldsymbol{\mu}_B = M_\mathrm{B} V_\mathrm{B} \begin{bmatrix} -1 \\ 0 \\ 0 \end{bmatrix}, \tag{47b}$$

where M_A and M_B represents the vector sum of all microscopic magnetic moments within a ferromagnetic material and V_A and V_B are the volumes of the magnets. Details of the force between magnetic dipoles can be found in [16]. ϕ is the rotation angle at the magnet A.

The vector from the source of magnet B to magnet A is

$$\mathbf{r}_{AB} = \begin{bmatrix} -\left(s + \frac{l_\mathrm{A}}{2} + \frac{l_\mathrm{B}}{2} + \left(l_\mathrm{P} + \frac{l_\mathrm{A}}{2}\right)(1 - \cos\phi)\right) \\ 0 \\ q \end{bmatrix} \tag{48}$$

where l_A and l_B are the length of the magnets and l_P is the length of the beam in x-direction.

Figure 12 a) presents the potential energy

$$U = U_\mathrm{mech} + U_\mathrm{mag} = \frac{1}{2} c q^2 + \frac{\mu_0}{4\pi} \left(\frac{\boldsymbol{\mu}_A \cdot \boldsymbol{\mu}_B}{r_{AB}^3} - 3 \frac{(\boldsymbol{\mu}_A \cdot \mathbf{r}_{AB})(\boldsymbol{\mu}_B \cdot \mathbf{r}_{AB})}{r_{AB}^5} \right) \tag{49}$$

where U_mech is the mechanical potential energy and c is the equivalent stiffness of the beam. U is normalized to the potential energy U_0 for a magnet distance of $s = 0.79 s_0$. The tip displacement q is normalized to the tip displacement q_0 for $s = 0$. The derivation of the mechanical potential energy expression is shown in [15] and is proportional to q^2 for the first bending mode. U_mag is given in Equation 45. The Figure shows the potential energy for different magnet distances with respect to s_0 which is the critical magnet distance where the potential energy change from two to one stable equilibrium position. The nonlinear magnetic

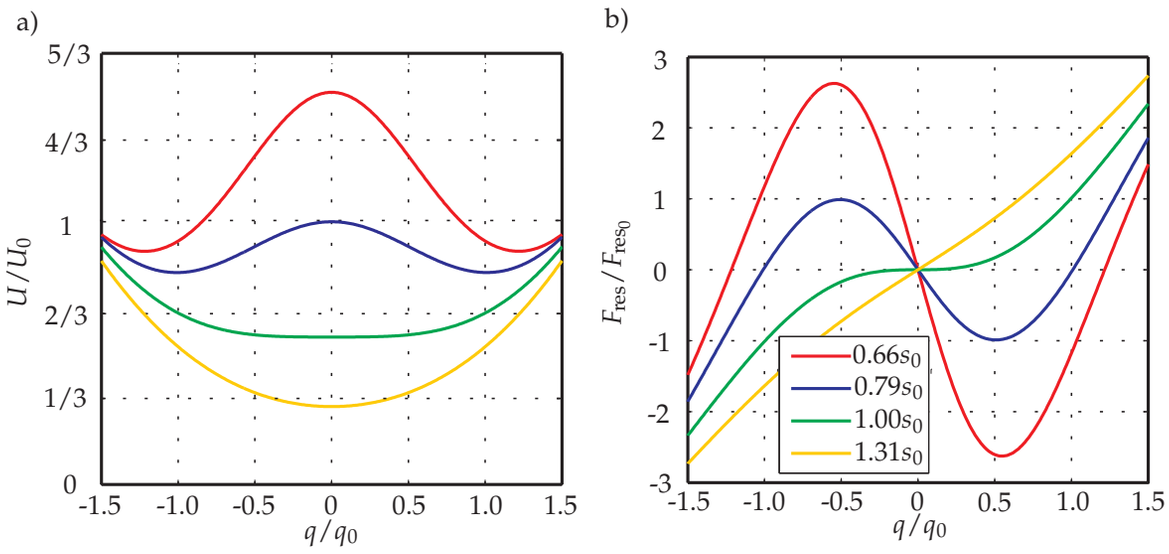

Figure 12. Potential energy and restoring force

force leads to an energy hump at zero tip displacement. A sharp peak results for a small spacing.

The system exhibits two stable equilibrium positions which are the local minimum positions in the potential energy and one unstable equilibrium for zero displacement ($s < s_0$). The hump disappears for large s and there is only one stable equilibrium for zero displacement ($s > s_0$).

The normalized restoring force

$$F_{\text{res}} = \frac{dU}{dq} \tag{50}$$

is additionally presented in Figure 12 b). F_{res} is normalized to the restoring force for a magnet spacing of $s = 0.79s_0$. Equation 50 is a nonlinear function of the system parameters in particular a function of s.

The benefit of the magnet force is the nonlinearity in the system response. Due to the restoring force the system exhibits overhanging resonance curves which strongly depends on the parameters. For $s < s_0$ and low excitation energy that the system only oscillates around one equilibrium the EOM has a hardening stiffness so the resonance curve overhang to the left. A softening response is given for $s > s_0$ with a distorted peak to the right. Specially for a hardening stiffness the system exhibit two equilibrium positions and the system bounces between both positions if the energy of the excitation is high enough. These large orbit deflections generate the most energy and are most important for designing the system setup.

5.2. Approximation with the Duffing oscillator

The potential energy shown in Figure 12 a) is approximated as fourth order polynomial function

$$U_{\text{Duff}} = \frac{1}{4}\alpha q^4 + \frac{1}{2}\beta q^2 \tag{51}$$

in a bunch of different research activities. The nonlinear restoring force shown in Figure 12 b) is than approximated as the Duffing equation

$$F_{\text{res,Duff}} = \frac{dU_{\text{Duff}}}{dq} = \alpha q^3 + \beta q \tag{52}$$

with the Duffing parameters α and β. The approach as Duffing equation is not only limited to piezomagnetoelastic energy harvesting techniques. [5] used this equation to model an electrostatic energy harvesting system and [8] approximate an electromagnetic energy generator. In the following α is the Duffing parameter before the cubic term instead of the coupling factor in Equation 43 to be conform to the most publications concerning the duffing equation. The uncoupled equation of motion (EOM) for the piezomagnetoelastic system in terms of the duffing oscillator is written as

$$m\ddot{q} + d\dot{q} + \alpha q^3 + \beta q = F(t). \tag{53}$$

The Duffing parameters are complicated functions of the beam, the piezo, the magnet parameters and in particular the magnet distance. It can be recognized in Figure 12 b) that the cubic part αq^3 is always positive for repulsive magnets because the function is always monotonically increasing for large q values. Only the linear part βq can be either positive or negative with respect to the magnet distance. For $s < s_0$ the parameter β is negative and the system exhibits two stable and one unstable equilibrium position. For $s \geq s_0$ the system has only one stable equilibrium position and β is positive. s_0 is the critical magnet spacing.

The nonlinear restoring force F_{res} shown in Figure 12 b) can be approximated as a third order Taylor serious given with

$$p(q) = k_1 q^3 + k_2 q^2 + k_3 q + k_4 \tag{54}$$

where k_{1-4} are constants derived from the system parameters. By comparing Equation 54 and Equation 52 note that $k_1 = \alpha$ and $k_3 = \beta$. To calculate the constant parameters in Equation 54 it takes four constrains.

1. The restoring force is point symmetric:

$$p(0) = 0, \tag{55}$$

$$\frac{d^2 p(0)}{dq^2} = 0. \tag{56}$$

2. The Taylor series must exhibit the same equilibrium positions:

$$p(q_{\text{eq}}) = 0. \tag{57}$$

3. The oscillation must be suitable for small magnet distances s around one equilibrium position

$$\frac{dp(q_{\text{eq}})}{dq} = a, \tag{58}$$

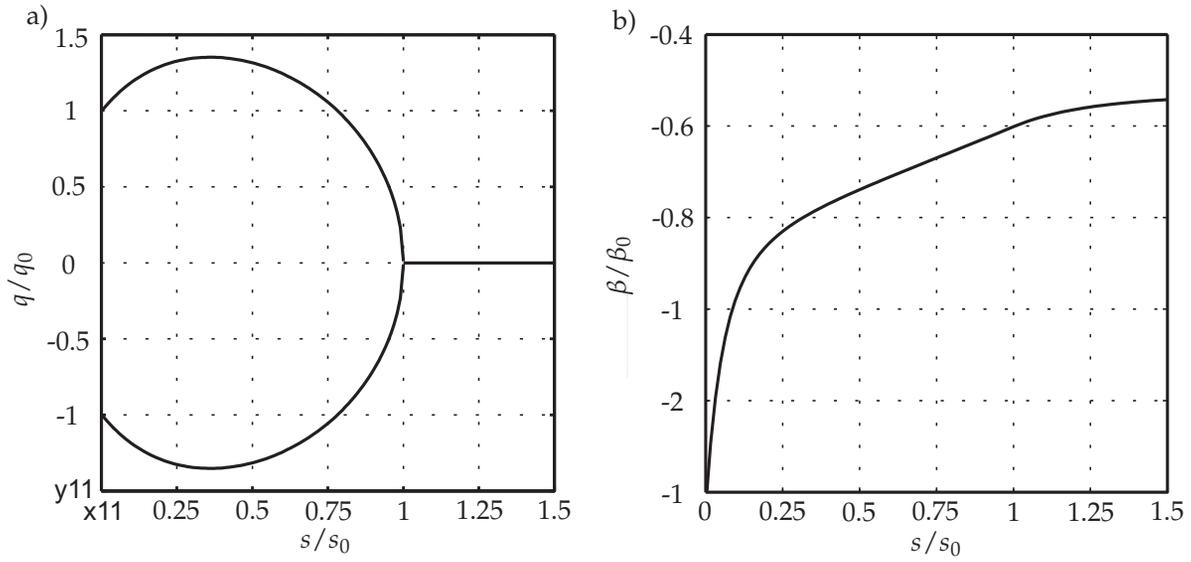

Figure 13. Equilibrium positions and β with respect to the magnet distance s.

where q_{eq} is the equilibrium position and a is the slope at q_{eq}. a and q_{eq} can be calculated from the original system. The solution for k_{1-4} is

$$k_1 = \alpha = \frac{a}{2q_{\text{eq}}^2}, \tag{59a}$$

$$k_2 = 0, \tag{59b}$$

$$k_3 = \beta = -\frac{a}{2}, \tag{59c}$$

$$k_4 = 0. \tag{59d}$$

Equation 53 becomes

$$m\ddot{q} + d\dot{q} + \frac{a}{2q_{\text{eq}}^2}q^3 - \frac{a}{2}q = F(t). \tag{60}$$

Equation 60 is usable if the potential energy exhibits two equilibrium positions. If the magnet distance is larger than s_0 the Duffing parameters α and β are simply the liner and the cubic part of the third order Taylor series of Equation 50 and α and β are positive.

This behavior can be recognized in Figure 13 a) and b). The graphs are calculated by using the potential energy of two point dipols in Equation 49. Figure a) shows the equilibrium position over the magnet distance. The equilibrium position q_{eq} is normalized to the known q_0. The magnet distance is normalized to the critical magnet distance s_0. Note that the distance between the two stable q_{eq} becomes smaller for very small s because of the rotation angle ϕ of magnet A. The Figure 13 b) gives the modification of the Duffing parameter β with respect to the normalized known magnet distance. β is normalized to β_0 the linear Duffing parameter

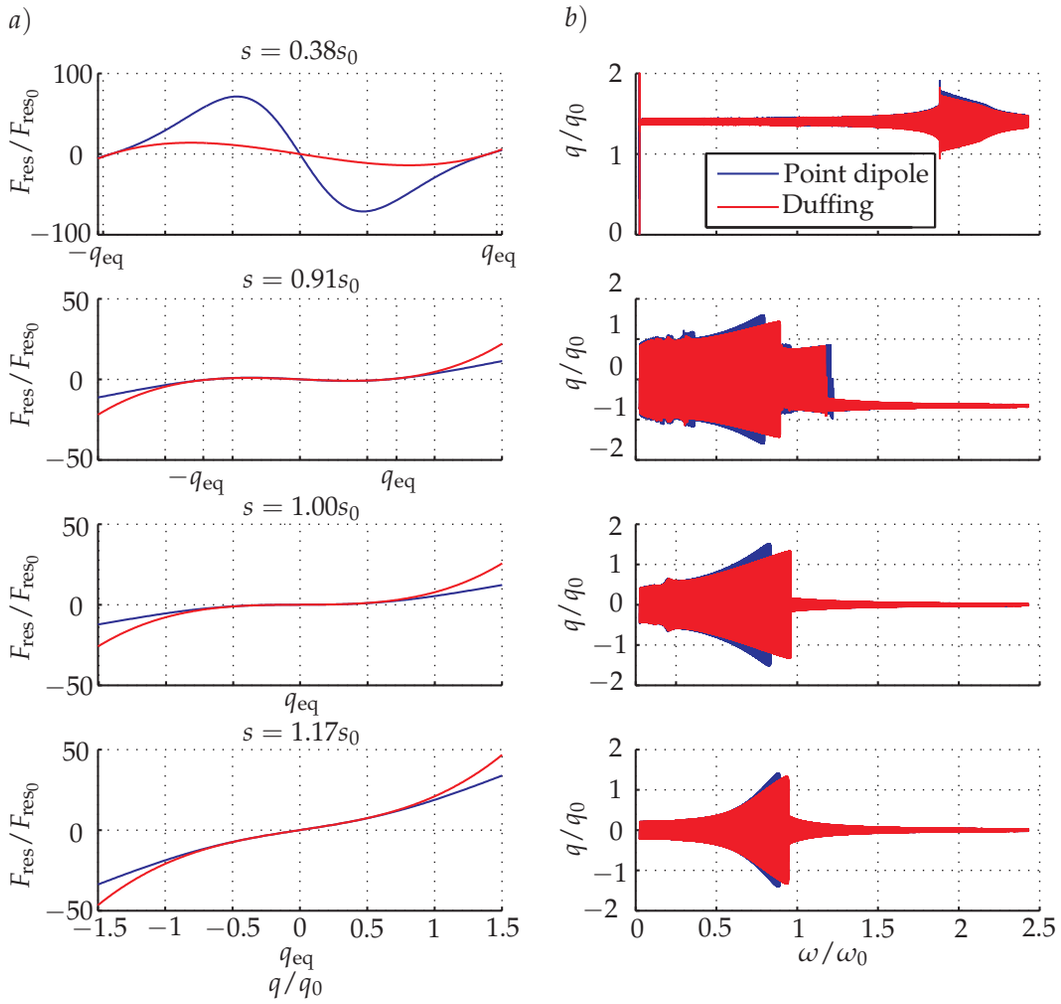

Figure 14. Duffing approximation of the restoring force and displacement

for $s = 0$. For $s < s_0$ the system exhibit a negative linear restoring force due to the negative parameter β. β is positive for $s > s_0$.

Figure 14 shows the approximation of Equation 50 with Equation 52 and the Duffing parameter known from Equation 59. The pictures a) show the restoring force derived from the force between two point dipoles and the Duffing equation for different magnet distances. The pictures b) gives the corresponding time variant tip displacement. It can be recognized that the Duffing equation approximate the restoring force very well for the different ranges of magnet spacing. The Duffing equation shows the hardening response for small magnet distances ($s = 0.38s_0$) and it approximates the influence of the different attractors ($s = 0.91s_0$). For $s > s_0$ the approximation is also very good.

5.3. Solution for large orbit oscillations

In Section 5.1 and Section 5.2 the piezomagnetoelastic energy harvesting system is presented and an approximation with the Duffing oscillator is given. In the following Equation 60 is

solved for large orbit oscillations so that system bounces between both symmetric equilibrium positions or around the only one for $s > s_0$. The EOM can be written as

$$\ddot{q} + 2D\omega_0\dot{q} + \epsilon q^3 + \mathrm{sgn}(\beta)\omega_0^2 q = f_0 \cos(\omega t) \tag{61}$$

where $\mathrm{sgn}(\beta)$ is either positive or negative for $\beta > 0$ or $\beta < 0$ with

$$D = \frac{d}{2\omega_0 m}, \tag{62a}$$

$$\omega_0^2 = \frac{|\beta|}{m}, \tag{62b}$$

$$\epsilon = \frac{\alpha}{m}, \tag{62c}$$

$$f_0 = \frac{\hat{F}}{m}. \tag{62d}$$

The Equation 61 can be solved by applying the harmonic balance method. The harmonic balance method is well known and details can be found in [12]. The amplitude response is assumed as harmonic with the frequency of the excitation

$$q = \hat{q}cos(\omega t - \varphi) \tag{63}$$

where $\hat{q}$ is the amplitude and φ is the phase of the tip displacement. Insert Equation 63 in Equation 61 and only consider terms with the excitation frequency leads to

$$\sqrt{\left[\left(\mathrm{sgn}(\beta)\omega_0^2 - \omega^2\right)\hat{q} + \frac{3}{4}\epsilon\hat{q}^3\right]^2 + 4D^2\omega_0^2\omega^2\hat{q}^2}\cos\left(\omega t - \ldots\right.$$

$$\left.\ldots - \varphi + \arctan\left(\frac{2D\omega_0\omega\hat{q}}{(\mathrm{sgn}(\beta)\omega_0^2 - \omega^2)\hat{q} + \frac{3}{4}\epsilon\hat{q}^3}\right)\right) = f_0\cos(\omega t). \tag{64}$$

The Equation 61 is valid if the amplitude and the phase in Equation 63 solves the equations. The solution gives the frequency response with respect to the amplitude $\hat{q}$

$$\omega_{1/2}^2 = \mathrm{sgn}(\beta)\omega_0^2 - 2D\omega_0^2 + \frac{3}{4}\epsilon\hat{q}^2 \pm \sqrt{\frac{f_0^2}{\hat{q}^2} + 4D^2\omega_0^2\left(D^2\omega_0^2 - \mathrm{sgn}(\beta)\omega_0^2 - \frac{3}{4}\epsilon\hat{q}^2\right)}. \tag{65}$$

Figure 15 shows the analytical amplitude response given in Equation 65 and the numerical solution of the Duffing oscillator. The graph shows the solution for three different magnet distances. The frequency was slowly increased so the system remains a steady state response. One can recognize that the harmonic balance is well suited if the Duffing equation has a positive linear restoring force ($\beta > 0$). If the Duffing oscillator exhibits a negative restoring force and the system excitation delivers enough energy that the energy harvester bounces between both stable equilibrium positions than the harmonic balance predicts the influence of

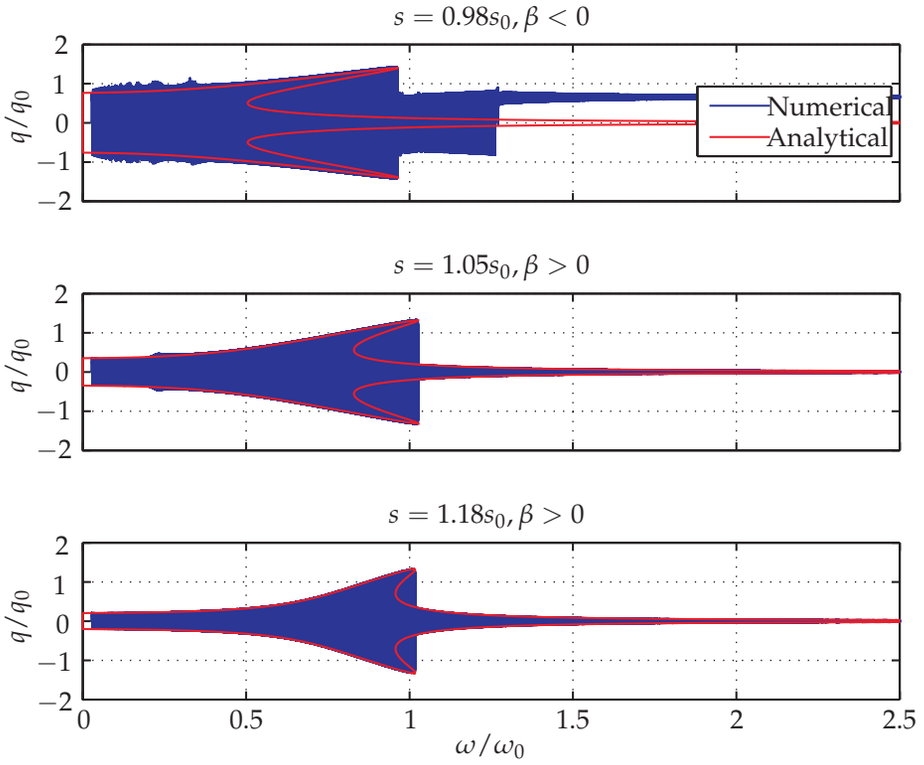

Figure 15. Numerical and analytical results for the large orbit duffing equation

the attractors till the first jump. The system behavior after the first jump can not be predicted with this harmonic approximation.

6. Conclusions

This chapter presents different techniques to enlarge the frequency bandwidth of piezoelectric energy harvester. A precise modeling of piezomechanical structures is given, and the linear harvesting system is given as the reference. In detail a nonlinear switching SSHI circuit, nonlinear magnet forces and an array configuration of several bimorphs are discussed. For all cases, appropriate modeling techniques are presented that allow an efficient yet precise analysis. The nonlinear techniques alter the system dynamics especially for off-resonance vibrations. The magnet forces generate a bistable system, in which the bimorph oscillates between both equilibria. The SSHI circuit increase the energy conversion rate by producing a rectangular shaped voltage signal, while the array configuration tunes the individual bimorphs to slightly different frequencies, so that the energy conversion is distributed to a broader frequency range.

Author details

Marcus Neubauer, Jens Twiefel, Henrik Westermann and Jörg Wallaschek
Leibniz University Hannover, Institute of Dynamics and Vibration Research, Appelstrasse 11, 30167 Hannover, Germany

7. References

[1] Erturk, A., Hoffmann, J. & Inman, D. [2009]. A piezomagnetoelastic structure for broadband vibration energy harvesting, *Applied Physics Letters* .

[2] Ferrari, M., Ferrari, V., Guizzetti, M., Andò, B., Baglio, S. & C.Trigona [2010]. Improved energy harvesting from wideband vibrations by nonlinear piezoelectric converters, *Sensors and Actuators A: Physical* .

[3] Guyomar, D., Badel, A., Lefeuvre, E. & Richard, C. [2005]. Toward energy harvesting using active materials and conversion improvement by nonlinear processing, *Ultrasonics, Ferroelectrics and Frequency Control, IEEE Transactions on* 52(4): 584–595.

[4] Guyomar, D., Magnet, C., Lefeuvre, E. & Richard, C. [2006]. Power capability enhancement of a piezoelectric transformer, *Smart Materials and Structures* 15(2): 571–580. URL: *http://stacks.iop.org/0964-1726/15/571*

[5] Halvorsen, E., Blystad, L.-C., Husa, S. & Westby, E. [2007]. Simulation of electromechanical systems driven by large random vibrations, *MEMSTECH*.

[6] *IEEE standard on piezoelectricity* [29 Jan 1988]. *ANSI/IEEE Std 176-1987* .

[7] Lallart, M., Guyomar, D., Richard, C. & Petit, L. [2010]. Nonlinear optimization of acoustic energy harvesting using piezoelectric devices, *Journal of the Acoustical Society of America* 128: 2739–2748.

[8] Mann, B. & Sims, N. [2009]. Energy harvesting from the nonlinear oscillations of magnetic levitation, *Journal of Sound and Vibration* 319: 515–530.

[9] Neubauer, M., Schwarzendahl, S. & Wallaschek, J. [2012]. A new solution for the determination of the generalized coupling coefficient for piezoelectric systems, *Journal of Vibroengineering* 14(1): 105–110.

[10] Neubauer, M. & Wallaschek, J. [2011]. Optimized geometry of bimorphs for piezoelectric shunt damping and energy harvesting, *Proceedings of Int. Conference of Engineering Against Fracture (ICEAF)*.

[11] Priya, S. & Inman, D. (eds) [2009]. *Energy Harvesting Technologies*, Springer.

[12] Schmidt, G. & Tondl, A. [1986]. *Non-Linear Vibrations*, Akademie-Verlag Berlin.

[13] Sebald, G., Kuwano, H., Guyomar, D. & Ducharne, B. [2011]. Experimental duffing oscillator for broadband piezoelectric energy harvesting, *Smart Materials and Structures* 20.

[14] Stanton, S., McGehee, C. & Mann, B. [2009]. Reversible hysteresis for broadband magnetopiezoelastic energy reversible hysteresis for broadband magnetopiezoelastic energy harvesting, *Applied Physics Letters* 95.

[15] Stanton, S., McGehee, C. & Mann, B. [2010]. Nonlinear dynamics for broadband energy harvesting: Investigation of a bistable piezoelectric inertial generator, *Physica D: Nonlinear Phenomena* .

[16] Yung, K., Landecker, P. & Villani, D. [1998]. An analytic solution for the force between two magnetic dipoles, *Magnetic and Electrical Separation* 9: 39–52.